Preprints.org

Article

Not peer-reviewed version

Evaluation of the Anticancer Effects of *Warburgia salutaris* Leaf Extracts: A Comparative Study of Both Liposomal-Encapsulated and Unencapsulated, with Mechanistic Insights into Apoptotic Signalling

Daniel M. Tswaledi , Matlou P. Mokgotho * , Makgwale S. Mphahlele , Raymond T. Makola , Jean B. Ngilirabanga , Bwalya A. Witika , Emelinah H. Mathe , Stanley S. Gololo , Ananias H. Kgopa , Leshweni J. Shai *

Posted Date: 25 March 2026

doi: 10.20944/preprints202603.1998.v1

Keywords: cancer; *Warbugia salutaris;* liposomes; cellular metabolic activity; Apoptosis

Preprints.org is a free multidisciplinary platform providing preprint service that is dedicated to making early versions of research outputs permanently available and citable. Preprints posted at Preprints.org appear in Web of Science, Crossref, Google Scholar, Scilit, Europe PMC.

Copyright: This open access article is published under a Creative Commons CC BY 4.0 license, which permit the free download, distribution, and reuse, provided that the author and preprint are cited in any reuse.

Preprints.org (www.preprints.org) | NOT PEER-REVIEWED | Posted: 25 March 2026 doi:10.20944/preprints202603.1998.v1

Disclaimer/Publisher's Note: The statements, opinions, and data contained in all publications are solely those of the individual author(s) and contributor(s) and not of MDPI and/or the editor(s). MDPI and/or the editor(s) disclaim responsibility for any injury to people or property resulting from any ideas, methods, instructions, or products referred to in the content.

Article

Evaluation of the Anticancer Effects of *Warburgia salutaris* Leaf Extracts: A Comparative Study of Both Liposomal-Encapsulated and Unencapsulated, with Mechanistic Insights into Apoptotic Signalling

Daniel M. Tswaledi [1], Matlou P. Mokgotho [2,*], Makgwale S. Mphahlele [3], Raymond T. Makola [4], Jean B. Ngilirabanga [5], Bwalya A. Witika [5], Emelinah H. Mathe [1], Stanley S. Gololo [1], Ananias H. Kgopa [1] and Leshweni J. Shai [3,*]

[1] Department of Biochemistry and Biotechnology, School of Science and Technology, Sefako Makgatho Health Sciences University, Pretoria 0204, South Africa

[2] Department of Physiology, School of Medicine, Sefako Makgatho Health Sciences University, Pretoria 0204, South Africa

[3] Department of Biomedical Sciences, Tshwane University of Technology, Pretoria 0183, South Africa

[4] Department of Biochemistry and Microbiology, University of Limpopo, Sovenga 0727, South Africa

[5] Department of Pharmaceutical Sciences, School of Pharmacy, Sefako Makgatho Health Sciences University, Pretoria 0204, South Africa

* Correspondence: phineas.mokgotho@smu.ac.za (M.P.M.); shailj@tut.ac.za (L.J.S.)

Abstract

Although medicinal plants possess vast biological properties, crude medicinal plant extracts often show limited therapeutic efficacy due to poor aqueous solubility, instability, and inadequate bioavailability, which restricts efficient intracellular delivery. As cancer is a genetic disease requiring intracellular and nuclear targeting, improved delivery systems are essential. *Warburgia salutaris* is traditionally used in Southern Africa and possesses reported anticancer and anti-inflammatory properties; however, its crude extracts exhibit suboptimal delivery characteristics. This study comparatively evaluated the anticancer effects of unencapsulated (WSN) and liposomal-encapsulated (WSE) crude leaf extracts, with emphasis on apoptotic mechanisms. Liposomal formulation was confirmed by FTIR, PXRD, and DLS, yielding stable nanoparticles (159.4 nm; PDI 0.114; +79.3 mV). Both WSN and WSE demonstrated efficacy, concentration-dependent cytotoxicity against MCF-7 breast cancer cells (IC_{50} < 0.0195 mg/mL) with minimal toxicity toward Vero kidney cells and Raw 264.7 macrophages. Mechanistically, WSN induced rapid cytotoxicity with necrotic features, whereas WSE promoted regulated apoptosis. Apoptosis was validated by DAPI/PI staining, Annexin V/PI flow cytometry, mRNA expression levels of Bax, Bcl-2, and caspase-3 measured with RT-PCR and proteome profiling array confirming activation of intrinsic and extrinsic pathways. Both extracts also reduced LPS-induced ROS production. LC-MS identified multiple bioactive phytochemicals. Overall, liposomal encapsulation enhanced therapeutic precision, stability, and selectivity cytotoxicity, supporting its development as a nanomedicine-based anticancer strategy.

Keywords: cancer; *Warbugia salutaris;* liposomes; cellular metabolic activity; Apoptosis

1. Introduction

Cancer is a non-communicable disease associated with significant morbidity and mortality worldwide. It is characterised by uncontrolled cell proliferation, metastatic progression, and resistance to apoptosis [1–3]. Despite advances in chemotherapy, immunotherapy, and targeted molecular therapies, effective cancer treatment remains limited by poor tumour selectivity, systemic

© 2026 by the author(s). Distributed under a Creative Commons CC BY license.

Preprints.org (www.preprints.org) | NOT PEER-REVIEWED | Posted: 25 March 2026 doi:10.20944/preprints202603.1998.v1

toxicity, therapeutic resistance and inadequate bioavailability of many anticancer agents [4–6]. These challenges are particularly pronounced in low- and middle-income regions, including sub-Saharan Africa, where delayed diagnosis and limited access to treatment contribute significantly to cancer-related mortality [7,8].

Natural products and plant-derived compounds continue to play a central role in anticancer drug discovery and development, providing structurally diverse bioactive molecules capable of modulating multiple cancer-associated pathways [9–11]. Several clinically used anticancer agents have originated from medicinal plants, highlighting the therapeutic relevance of phytochemicals [12,13]. Plant-derived compounds have been shown to regulate key cellular processes, including cell-cycle arrest, oxidative stress modulation, mitochondrial dysfunction and induction of apoptosis [14–16]. Despite promising in vitro activity, many crude plant extracts exhibit limited clinical translation due to poor aqueous solubility, instability, and inefficient intracellular delivery [17,18].

Warburgia salutaris (Canellaceae), commonly known as the pepper-bark tree, is an indigenous Southern African medicinal plant widely used in traditional medicine for the treatment of inflammation, infections, and tumour-related conditions [19–21]. *Warburgia salutaris* phytochemicals analysis has demonstrated a plethora of bioactive compounds, including sesquiterpenes, flavonoids, lignans, diarylheptanoids, and related secondary metabolites with reported cytotoxic, anticancer, and anti-inflammatory properties [22–25]. Previous studies have demonstrated that extracts of *W. salutaris* exhibit significant cytotoxic effects against various cancer cell lines. However, these effects are often accompanied by limited selectivity and non-specific cytotoxicity when administered as crude formulations [26,27].

Nanotechnology-based drug delivery systems have emerged as promising tools to overcome the limitations associated with conventional phytochemical delivery by improving solubility, stability, and intracellular uptake [28–30]. Among these systems, liposomes are particularly attractive due to their biocompatibility and ability to encapsulate both hydrophilic and hydrophobic compounds. Moreover, they are capacity to enhance therapeutic potency while reducing systemic toxicity [31–33]. Importantly, liposomal encapsulation has been shown to modulate cancer cell death pathways, shifting cytotoxic responses from immune-triggering necrosis toward regulated apoptosis, thereby overcoming inflammation and off-target tissue damage [34–36].

Apoptosis is a highly regulated form of programmed cell death that plays a critical role in maintaining tissue homeostasis and eliminating damaged or malignant cells [37,38]. Dysregulation of apoptotic signalling pathways is a cancer pathogenesis leading to tumour progression and therapeutic resistance [39,40]. Apoptotic cell death may be initiated through intrinsic (mitochondrial-mediated) or extrinsic (death receptor-mediated) pathways, both of which converge on the activation of executioner caspases such as caspase-3 [41–43]. Therapeutic strategies that restore or enhance apoptotic signalling are therefore considered central to effective anticancer intervention [44,45].

In addition to apoptosis resistance, chronic inflammation and excessive reactive oxygen species (ROS) production contribute to tumour initiation, progression, and metastasis [46,47]. During an inflammatory response macrophage-elicits ROS production, which can promote a tumour-supportive microenvironment [48]. Consequently, agents capable of simultaneously inducing apoptosis in cancer cells while suppressing inflammation-associated ROS production may offer enhanced therapeutic benefit [49,50]. Despite the documented biological activity of *W. salutaris*, the impact of the nanocarrier on drug delivery in an attempt to enhance anticancer potency is underexplored [51].

Therefore, the present study aimed to comparatively evaluate the anticancer effects of unencapsulated and liposomal-encapsulated *Warburgia salutaris* crude leaf extracts, with specific emphasis on apoptotic pathway activation, selective cytotoxicity and oxidative stress modulation.

2. Results

2.1. Phytochemical Characteristics Analysed by FTIR

© 2026 by the author(s). Distributed under a Creative Commons CC BY license.

Preprints.org (www.preprints.org) | NOT PEER-REVIEWED | Posted: 25 March 2026 doi:10.20944/preprints202603.1998.v1

FTIR spectroscopy was used to characterise functional groups and assess interactions between the *W. salutaris* crude extract, blank liposomes, and encapsulated liposomes (Figure 1A). The crude extract exhibited a broad O–H stretching band centred at ~3300 cm^{-1}, consistent with hydroxyl groups of phenolic constituents and residual moisture. A moderate absorption band near 1680 cm^{-1} corresponded to C=O stretching of aldehydes and ketones, while signals within 1450–1600 cm^{-1} were attributed to aromatic C=C stretching vibrations. Prominent C–O stretching bands between 1000–1300 cm^{-1} indicated the presence of alcohols and ether functionalities typical of phytochemicals.

The blank liposomes displayed characteristic lipid-associated bands, including aliphatic C–H stretching (2850–2950 cm^{-1}), ester C=O stretching (1735 cm^{-1}), and phosphate group vibrations at 1230 cm^{-1} (P=O) and 1080 cm^{-1} (P–O–C). The encapsulated formulation exhibited combined spectral features of both the extract and lipid components. The persistence of the O–H band and slight shifts and broadening of C=O and phosphate peaks relative to blank liposomes indicate molecular interactions between extract constituents and the lipid bilayer.

2.2. Powder X-Ray Diffraction (PXRD)

PXRD analysis was conducted to evaluate structural characteristics (Figure 1B). The crude extract showed a broad diffuse halo centred around 20° 2θ, confirming its amorphous nature. Blank liposomes composed of DPPC and cholesterol exhibited sharp diffraction peaks between 10° and 40° 2θ, indicative of a semi-crystalline lipid bilayer structure. The encapsulated formulation displayed a superimposed pattern comprising the amorphous halo of the extract and the crystalline reflections of the lipid matrix, demonstrating successful incorporation of the extract without disruption of lipid crystallinity.

2.3. Particle Size and Zeta Potential

Dynamic light scattering analysis (Table 1) revealed that the optimised encapsulated formulation had a mean particle size of 159.4 nm with a narrow size distribution (PDI = 0.114). The liposomes exhibited a high positive zeta potential of +79.3 mV. These parameters confirm the formation of nanosized, monodisperse vesicles with strong electrostatic stability, supporting colloidal integrity and resistance to aggregation.

Table 1. Physicochemical Characterisation of Optimised *W. salutaris* leaf extracts-loaded liposomes.

Parameter	Value	Comments
Average Particle size (nm)	159.4	Nanoscale vesicle suitable for drug delivery
Polydispersity Index (PDI)	0.114	A narrow size distribution indicates a monodisperse vesicle population
Zeta potential (mV)	+79.3	Strong positive surface charge, strong electrostatic repulsion, enhances colloidal stability and prevents aggregation

© 2026 by the author(s). Distributed under a Creative Commons CC BY license.

Preprints.org (www.preprints.org) | NOT PEER-REVIEWED | Posted: 25 March 2026 doi:10.20944/preprints202603.1998.v1

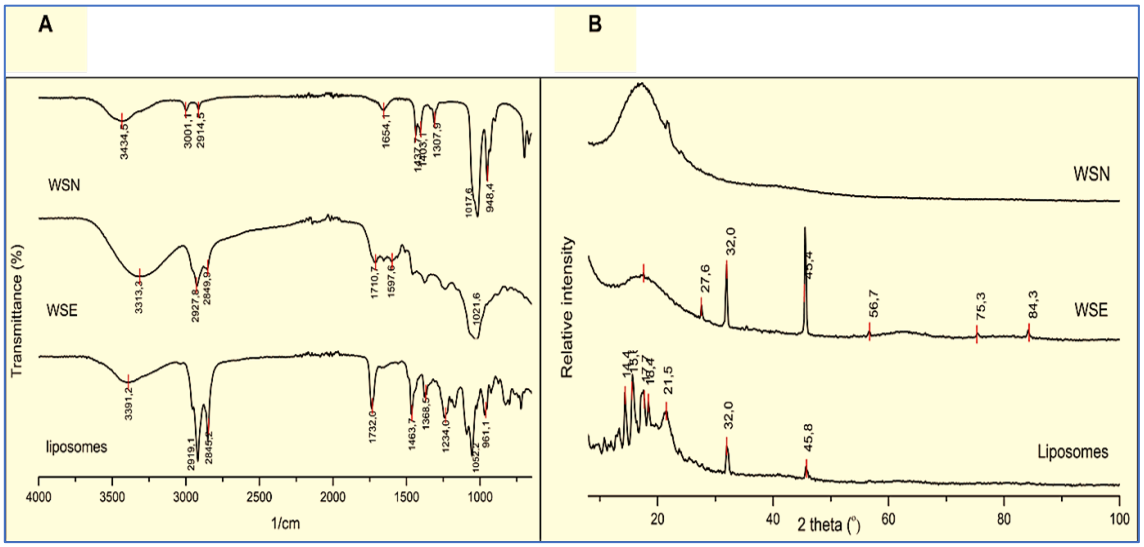

Figure 1. (A) Displays the FTIR spectra of *W. salutaris* unencapsulated (WSN), liposomal-encapsulated (WSE) crude leaf extracts and liposomes. (B) Presents the Powder X-ray diffraction (pXRD) analysis of the three samples mentioned above.

2.4. MTT Assay

The cytotoxic effects of WSN and WSE were evaluated using the MTT viability assay following 24 h exposure on MCF-7 breast cancer cells, Vero kidney epithelial cells, and RAW 264.7 macrophages (Figure 2). In MCF-7 cells (A), both extracts induced a significant, concentration-dependent reduction in metabolic activity across 0.0195–0.3125 mg/mL relative to untreated controls. Cell viability declined below 50% within this range, with IC_{50} values < 0.0195 mg/mL. The magnitude of cytotoxicity was comparable to the positive control, doxorubicin, which similarly produced a marked decrease in cell viability. In Vero cells (B), WSN and WSE demonstrated substantially lower cytotoxicity. IC_{50} values were markedly higher than those observed in MCF-7 cells, and cell viability remained above 75% across all tested concentrations. Statistical analysis revealed only minor differences compared with untreated controls. In contrast, doxorubicin significantly reduced metabolic activity in Vero cells (*** $p \leq 0.001$). In Raw 264.7 macrophages (C), exposure to WSN and WSE (1-0.063 mg/mL) did not significantly alter metabolic activity relative to controls, and no IC_{50} values were reached within the tested range. Conversely, hydrogen peroxide significantly decreased cell viability (**** $p \leq 0.0001$), confirming assay sensitivity. Collectively, these data demonstrate potent and selective cytotoxicity of WSN and WSE toward MCF-7 cells, with minimal effects on non-cancerous Vero cells and immune-derived Raw 264.7 macrophages.

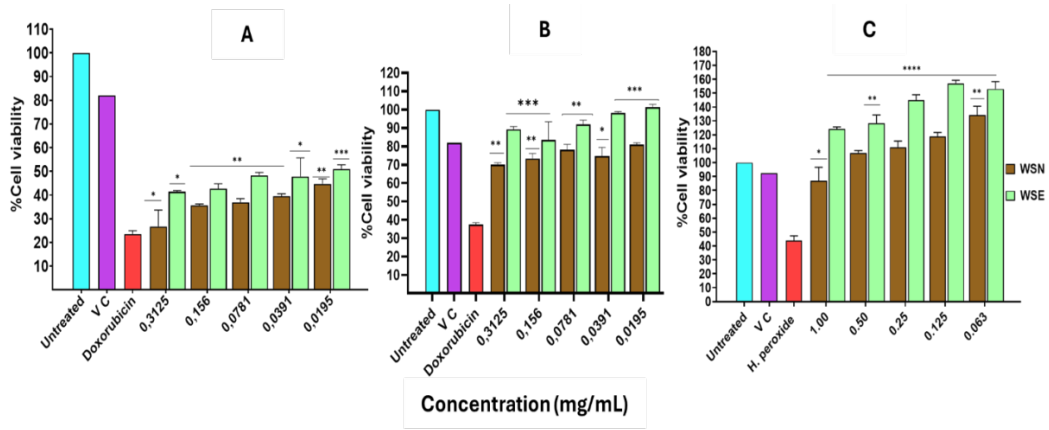

Figure 2. Cytotoxic effects of WSN and WSE extracts using the MTT assay. The cytotoxicity was evaluated after 24 hours of treatment with WSN and WSE extracts. The MCF-7 (A) and Ver (B) cells were treated with different

© 2026 by the author(s). Distributed under a Creative Commons CC BY license.

Preprints.org (www.preprints.org) | NOT PEER-REVIEWED | Posted: 25 March 2026 doi:10.20944/preprints202603.1998.v1

concentrations ranging from 0.3125 to 0.0195 mg/mL, and doxorubicin served as the positive control. Raw 264.7 cells were treated with concentrations ranging from 1 to 0.063 mg/mL, with hydrogen peroxide used as a positive control. Untreated cells served as the negative control, and DMSO was used as the vehicle control (VC). Data represent the mean ± standard deviation of two independent experiments, with * $p \leq 0.05$, ** $p \leq 0.01$, *** $p \leq 0.001$, and **** $p \leq .0001$ indicating significant differences compared to the control group.

2.5. Anti-Metastatic Effect on MCF-7 Cells Treated with WSN and WSE Leaf Extracts

The antimetastatic potential of WSN and WSE was evaluated using a scratch assay in MCF-7 cells (Figure 3). Representative micrographs captured at 0 and 24 h following treatment are shown in Figure 3A. Cells were treated with 0.3 mg/mL of WSN, WSE, or doxorubicin, with untreated cells serving as the negative control and doxorubicin as the positive control. At 24 h, untreated cells exhibited partial closure of the scratch area, indicating active cell migration. In contrast, treatment with doxorubicin markedly inhibited wound closure, confirming suppression of migratory capacity. Similarly, both WSN- and WSE-treated cells demonstrated significant inhibition of scratch closure compared to the untreated control. The wound area remained largely open after 24 h, reflecting impaired cell migration.

Quantitative analysis of the scratch area (Figure 3B) corroborated the microscopic observations. All treated groups showed a significant reduction in wound closure relative to untreated cells, indicating inhibition of migratory behaviour. The extent of migration inhibition observed with WSN and WSE was comparable to that of doxorubicin under the experimental conditions.

These findings demonstrate that both unencapsulated and liposome-encapsulated *W. salutaris* crude leaf extracts effectively suppress MCF-7 cell migration in vitro.

© 2026 by the author(s). Distributed under a Creative Commons CC BY license.

Preprints.org (www.preprints.org) | NOT PEER-REVIEWED | Posted: 25 March 2026 doi:10.20944/preprints202603.1998.v1

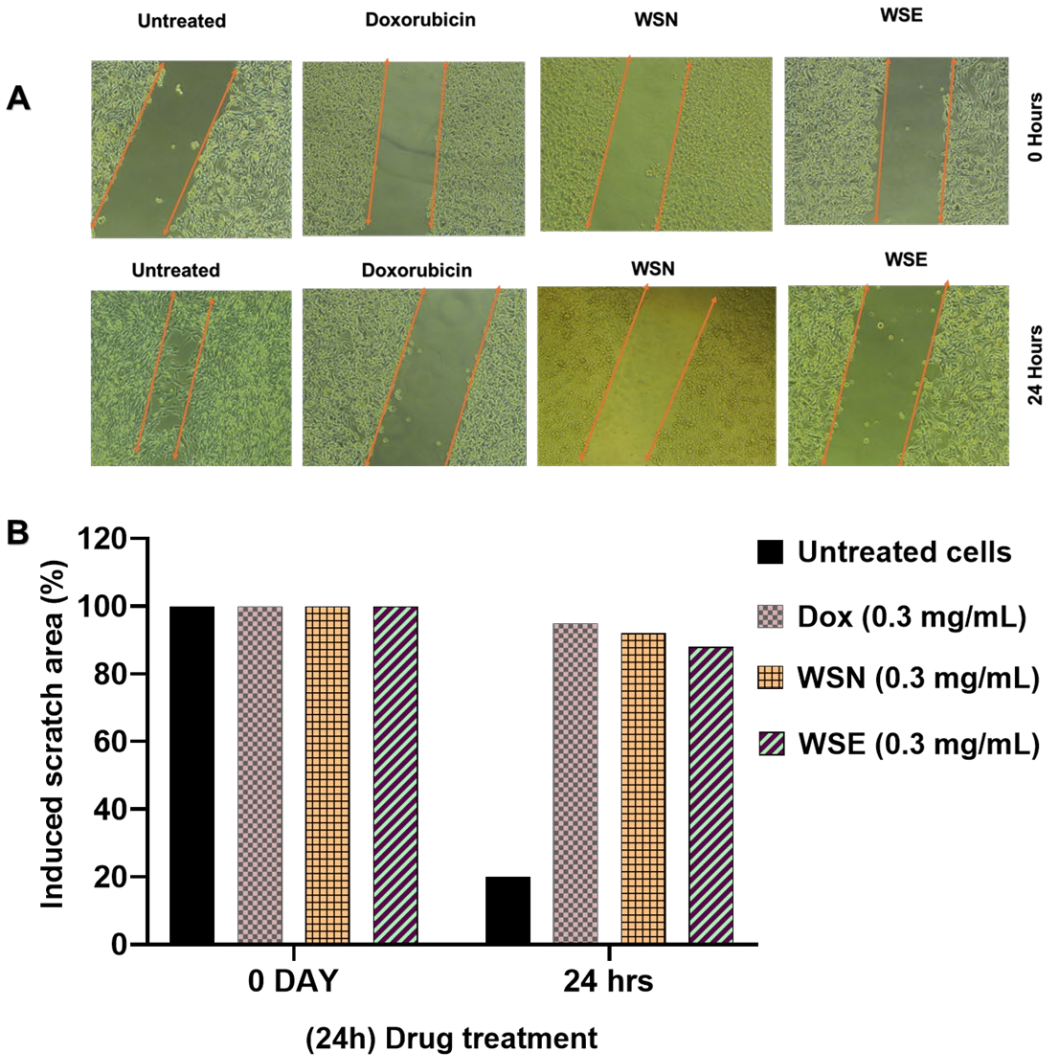

Figure 3. (A) Scratch assay images demonstrating anti-mitotic effects and (B) a graphical representation of the percentage of the scratched area in MCF-7 cells after treatment with WSN and WSE extracts, evaluated after 24 hours of exposure. Doxorubicin served as a positive control, while untreated cells acted as a negative control.

2.6. Determination of W. salutaris Induced Apoptotic Features Using DAPI/PI Staining

Induced mode of cell death on MCF-7 cells was evaluated using dual DAPI/PI staining following treatment with WSN, WSE (0.3 mg/mL), and doxorubicin (positive control) (Figure 4). Untreated cells exhibited intact nuclei with uniform DAPI staining and slight PI uptake, indicating preserved membrane integrity. Doxorubicin showed intense DAPI fluorescence with marked nuclear condensation, accompanied by strong PI staining, confirming late apoptosis. Cells treated with WSN and WSE extracts exhibited nuclear condensation and chromatin margination, which were confirmed by stronger DAPI fluorescence signals compared with the control samples. PI-positive cells were observed in both treatment groups, confirming membrane permeabilisation. Fluorescence intensity analysis indicated apoptotic induction in both groups, with WSN displaying stronger overall fluorescence relative to WSE. Brightfield microscopy further revealed morphological alterations in treated cells, including reduced cell density, cellular shrinkage, and structural disintegration, consistent with apoptotic progression. WSN and WSE induce nuclear condensation, chromatin margination, and membrane permeabilisation in MCF-7 cells, confirming apoptosis, with WSN showing slightly stronger effects than WSE.

© 2026 by the author(s). Distributed under a Creative Commons CC BY license.

Preprints.org (www.preprints.org) | NOT PEER-REVIEWED | Posted: 25 March 2026 doi:10.20944/preprints202603.1998.v1

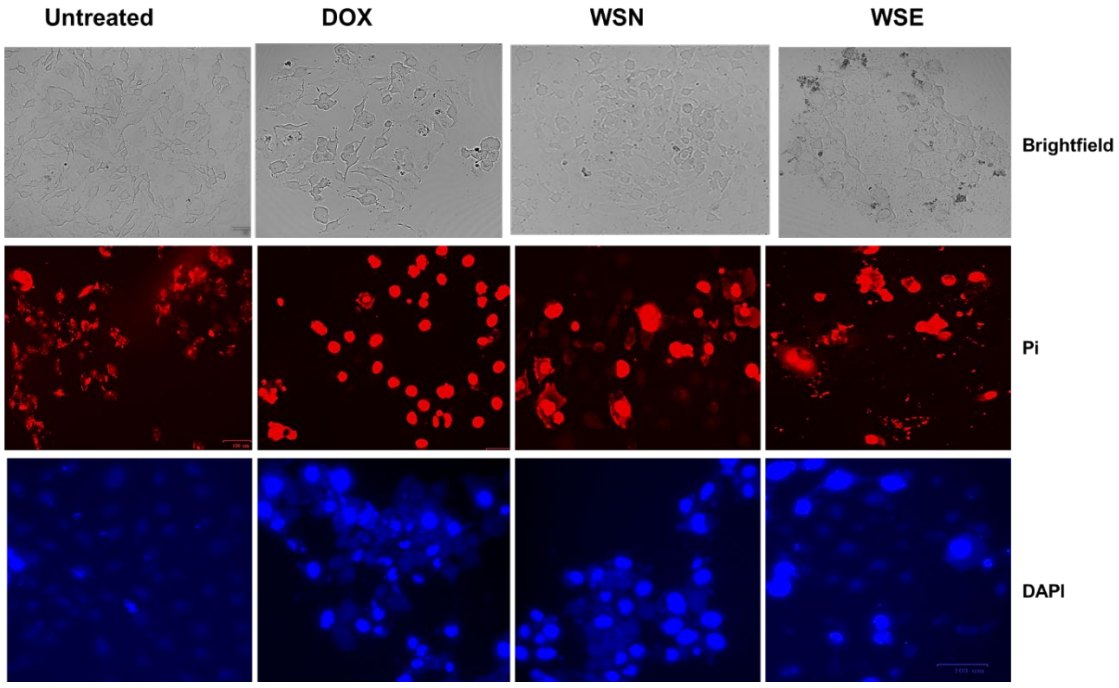

Figure 4. Brightfield and fluorescent images of MCF-7 cells stained with PI and DAPI after a 24-hour incubation with 0.3 mg/ml of crude unencapsulated WSN and liposomal-encapsulated WSE leaf extracts of *W. salutaris*. Doxorubicin hydrochloride served as the positive control, while untreated cells acted as the negative control.

2.7. Apoptotic Gene Expression Levels in MCF-7 Cells Analysed by RT-PCR

Reverse Transcription (RT-PCR) was used to evaluate gene expression on MCF-7 cells post exposure to *W. salutaris*, focusing specifically on pro-apoptotic and anti-apoptotic genes that include *Bax*, *Bcl-2*, and *caspase 3*. The *GAPDH* served as the reference gene. Gel electrophoresis was used to visualise the PCR amplicons. Figure 5A depicts the expressed bands alongside Figure 5B, which was used to illustrate the expression levels of each gene graphically. The findings indicate that the pro-apoptotic gene *Bax* increased the expression of *caspase 3*, while *Bcl-2* was downregulated following treatment. Figure 5B graphically supported the data, showing high percentages of the pro-apoptotic gene expression compared to anti-apoptotic genes in both the WSN and WSE.

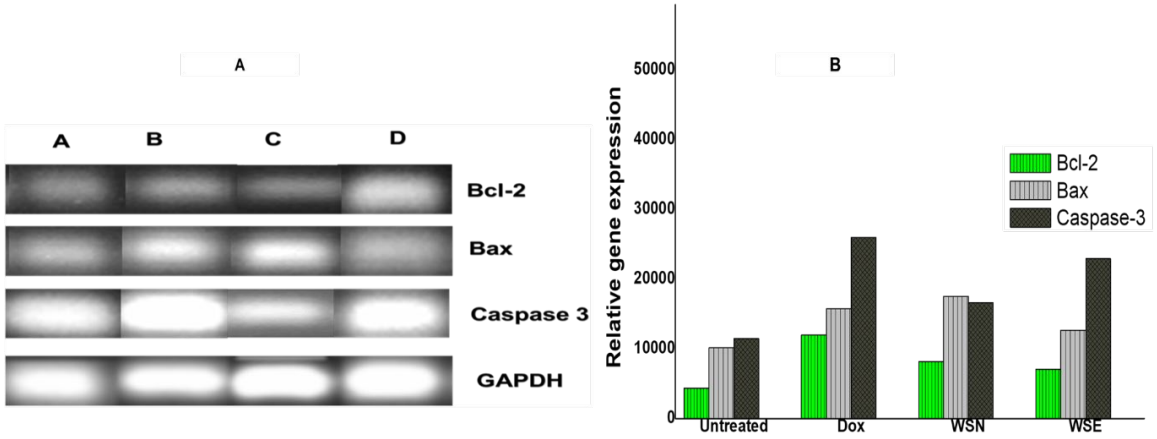

Figure 5. (A) Bands depicting expression levels of the apoptosis-related genes Bax, *Bcl-2*, *caspase-3*, and *GAPDH* were analysed after amplification using PCR. Gel electrophoresis was performed, producing the bands, and Zeo fluorescent microscopes were used to visualise them. The legend in the images indicates: 1: untreated control, 2: Doxorubicin as a positive control, 3: WSN, and 4: WSE crude leaf extracts. (B) The graph illustrates the percentage band intensity of the expression levels of apoptosis-associated genes. The data represent the mean

© 2026 by the author(s). Distributed under a Creative Commons CC BY license.

Preprints.org (www.preprints.org) | NOT PEER-REVIEWED | Posted: 25 March 2026 doi:10.20944/preprints202603.1998.v1

and standard deviation of the experiment. A *p*-value below 0.05 indicates that the results are statistically different from the negative control (untreated).

2.8. Analysis of the Human Apoptotic Proteome Profiling

The human apoptotic proteome profiler detected multiple proteins associated with apoptosis, indicating that apoptosis was activated in MCF-7 cells treated with 1 mg/ml of unencapsulated WSN and liposomal-encapsulated WSE leaf extracts through protein profiling. Both extracts increased the expression of *Bax, Bad, cleaved caspase-3, SMAC/Diablo, TRAIL R1/DR4, TRAIL R2/DR5, TNF RI, Fas/CD95, FADD,* and *phosphorylated p53 (S15, S46, S392), while reducing Bcl-2 and pro-caspase-3* levels. Notably, both extracts markedly induced cytochrome c release, representing a key event in mitochondrial-mediated apoptosis (Figure 6A). The pixel density of the expressed apoptotic proteins was shown in Figure 6B), supporting the indication of the bend intensity. In contrast, doxorubicin did not exhibit comparable cytochrome c expression under the tested conditions. WSN and WSE trigger both intrinsic (mitochondrial) and extrinsic apoptotic pathways, as evidenced by cytochrome c release and activation of key apoptotic proteins.

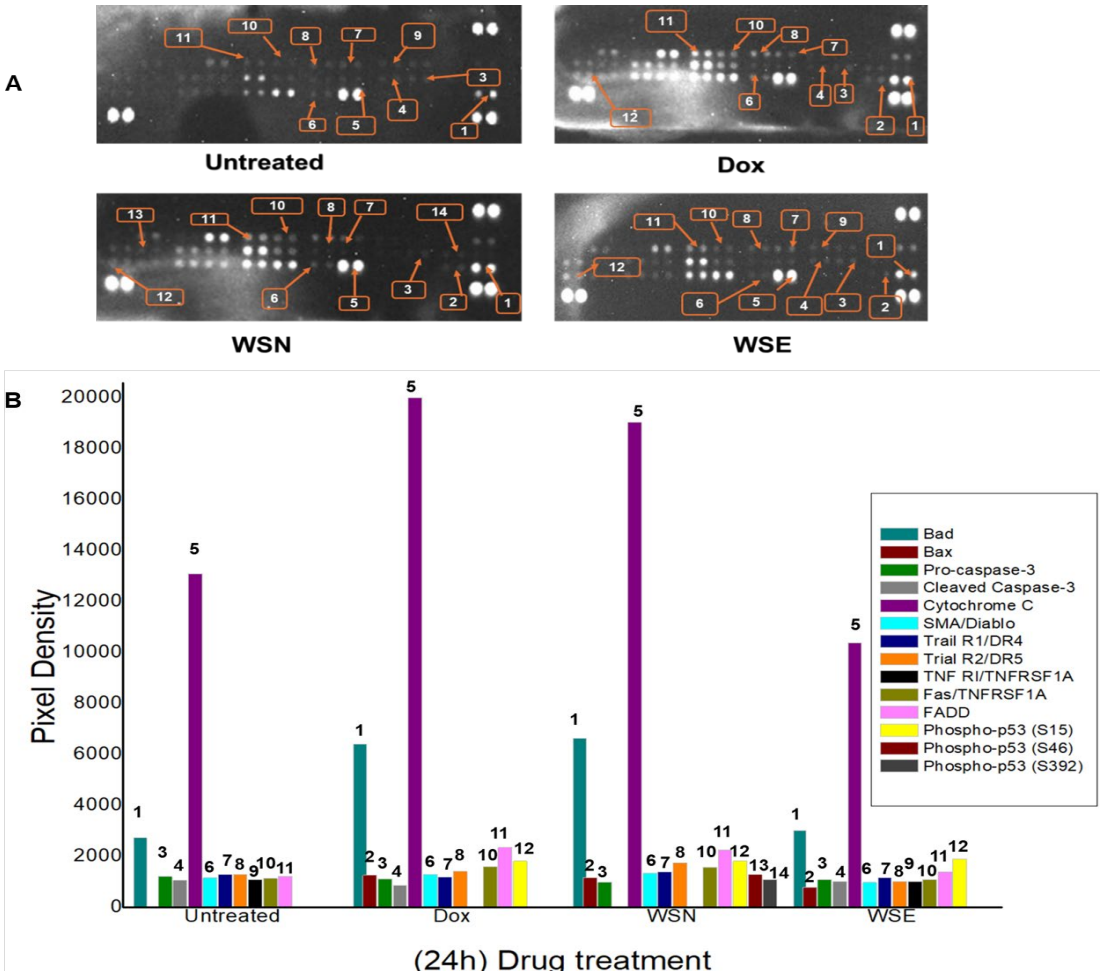

Figure 6. Images of pixel density produced by human apoptotic proteins expressed in MCF-7 cells. Doxorubicin hydrochloride served as the positive control, while untreated cells acted as the negative control. A total of 14 pro-apoptosis proteins were observed using ChemDoc Visualiser (A), and the percentage intensity of the pixels produced (B). The data represent the mean ± standard deviation of the experiment, with asterisks indicating significance levels (*$p < 0.05$, **$p < 0.01$, ***$p < 0.001$, ****$p < 0.0001$, and ns for not significant), demonstrating statistically significant differences compared to the negative control (untreated).

2.9. Analysis of Apoptosis Profile in MCF-7 Using the Annexin V/PI Staining Method

© 2026 by the author(s). Distributed under a Creative Commons CC BY license.

Preprints.org (www.preprints.org) | NOT PEER-REVIEWED | Posted: 25 March 2026 doi:10.20944/preprints202603.1998.v1

Figure 7 (A) shows the analysis of Annexin V/PI staining using the Muse® Cell Analyser, confirming that treating MCF-7 cells with unencapsulated (WSN) and liposomal-encapsulated (WSE) crude leaf extracts at 0.3 mg/mL for 24 hours induced increased late apoptosis. Untreated cells served as a negative control, while doxorubicin acted as a positive control, showing the highest activation of late apoptosis. Both WSN and WSE extracts resulted in low levels of apoptosis. The WSN extract showed robust cell death compared to the apoptosis process. The WSE extract induced apoptosis, as indicated in the late apoptosis quadrant. Figure (B) highlights that apoptosis was activated in a controlled manner, and late apoptosis showed higher values than early apoptosis. Liposomal encapsulation in WSE favours regulated apoptotic cell death, whereas free WSN indicated direct cell killing, which can lead to necrosis, highlighting the benefit of controlled delivery for therapeutic purposes

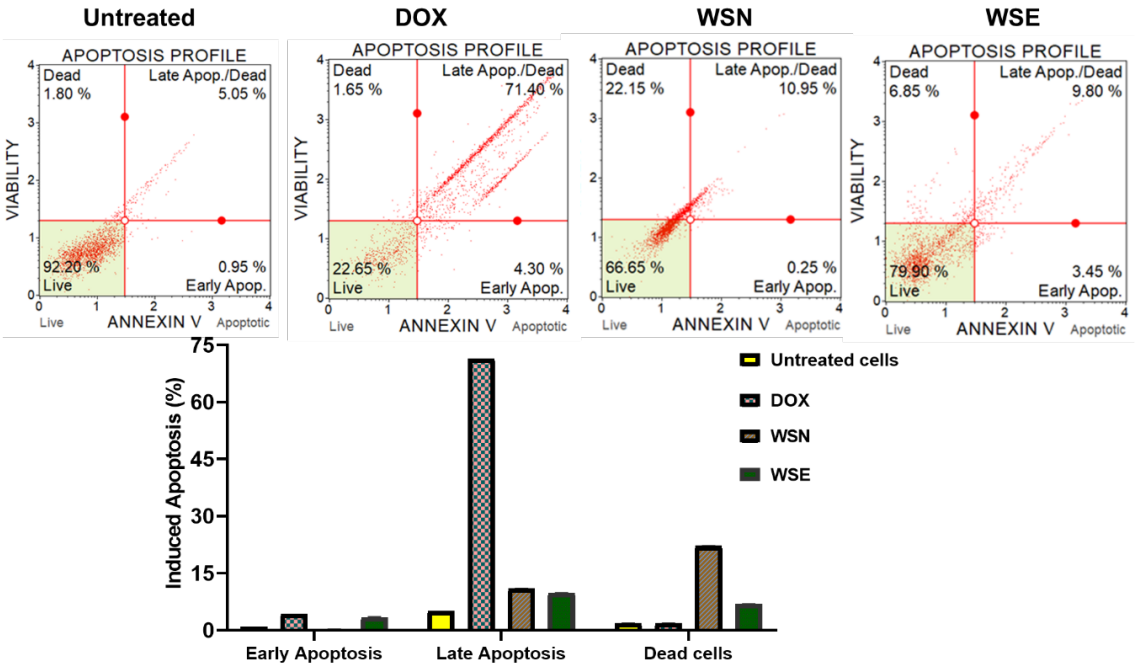

Figure 7. (A) displays images showing the effects of treatments on MCF-7 cells by inducing a type of cell death at a dose of 0.3 mg/ml of unencapsulated WSN and liposomal-encapsulated WSE leaf extracts. Doxorubicin hydrochloride served as the positive control, while untreated cells acted as the negative control. Muse® Cell Analyse was used to analyse the treated cells, which were categorised into four quadrants: 1) live, 2) early apoptosis, 3) late apoptosis, and 4) dead cells. (B) Shows the percentage of cell death.

2.10. The Effect of WSN and WSE Crude Leaf Extract on ROS Production Measured with H_2DCF-DA (ROS Probe)

The H_2DCF-DA assay was used to measure reactive oxygen species (ROS) production induced by lipopolysaccharide (LPS) in Raw 264.7 macrophages treated with unencapsulated (WSN) and liposomal-encapsulated (WSE) crude leaf extracts at a concentration of 0.125 mg/ml. This assay relies on the reaction of H_2DCF with ROS, which produces fluorescent DCF. The fluorescence intensity correlates with the amount of ROS generated. The Zoe fluorescence images, shown in Figure 8A, confirmed these results, demonstrating that LPS stimulated some cells to emit green fluorescence in both WSN and WSE treatments. However, imaging of WSE indicated a slightly significant reduction compared to the WSN. Both extracts showed the potential of inhibiting LPS-induced ROS production. Figure 8B presents the results graphically, indicating that cells treated with LPS exhibited significant green fluorescence, reflecting increased ROS levels compared to untreated controls. LPS significantly raised ROS production to over 82% relative to controls, demonstrating notable oxidative stress. Both

© 2026 by the author(s). Distributed under a Creative Commons CC BY license.

Preprints.org (www.preprints.org) | NOT PEER-REVIEWED | Posted: 25 March 2026 doi:10.20944/preprints202603.1998.v1

WSN and WSE crude leaf extracts markedly reduced ROS levels, with WSN-treated cells showing approximately a 68% decrease and WSE-treated cells around 64%.

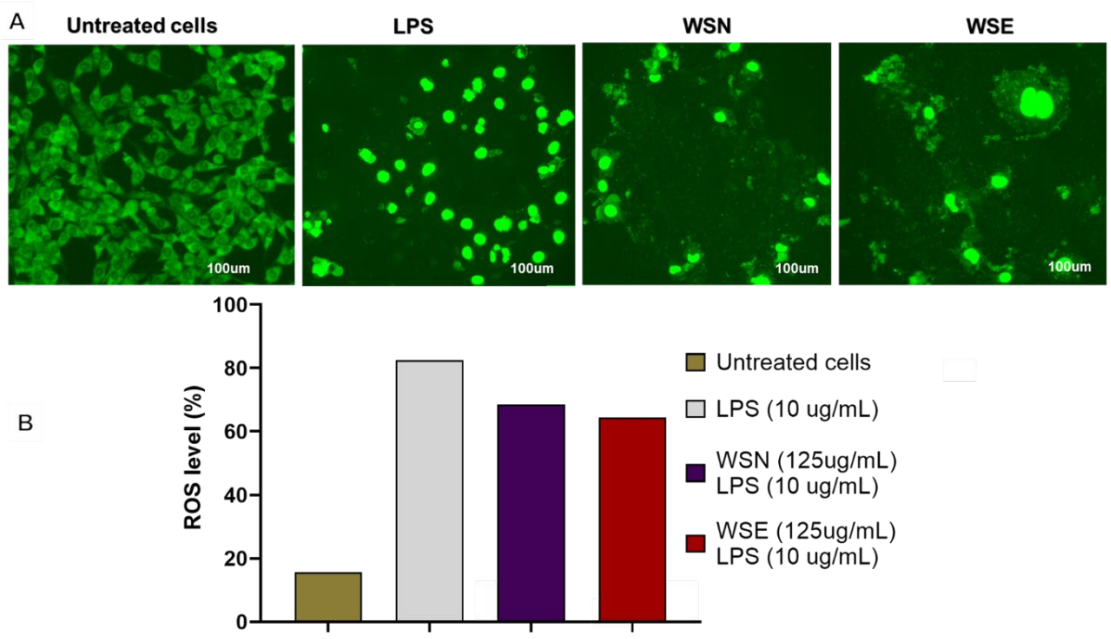

Figure 8. (A) The H2DCF-DA assay displays images illustrating the suppression of LPS-induced ROS after treatment. (B) The graph shows that cells treated with LPS exhibited significant green fluorescence, indicating increased ROS levels compared to untreated controls. The images depict the effect of LPS-induced ROS generation by extracts, captured using Zoe fluorescent microscopy with the H2DCF-DA dye.

2.11. Liquid Chromatography-Mass Spectrometry (LC-MS)

The LC-MS chromatogram of the crude leaf extract of *W. salutaris* prepared with equal parts of dichloromethane and methanol (50:50) displays a broad spectrum of secondary metabolites eluting between 4.47 and 13.94 minutes. Table 2 lists the twenty-four compounds identified based on their retention time (Rt), mass-to-charge ratio (m/z), chemical formula, and biological activities. Figure 9 shows the phytochemicals identified in the plant, including flavonoids (such as aurones, prenylated flavans, 8-O-methylated flavonoids, and flavonoid glycosides), lignans, biflavonoids, diarylheptanoids, anthracenes, naphthacenes, naphthopyrans, and curcuminoids, among others. Many of these compounds are associated with established anticancer, cytotoxic, and anti-inflammatory activities (Table 2). The LC-MS profile demonstrates that *W. salutaris* contains a chemically diverse array of bioactive compounds, supporting its observed apoptotic, antioxidant, and anti-inflammatory activities.

© 2026 by the author(s). Distributed under a Creative Commons CC BY license.

Preprints.org (www.preprints.org) | NOT PEER-REVIEWED | Posted: 25 March 2026 doi:10.20944/preprints202603.1998.v1

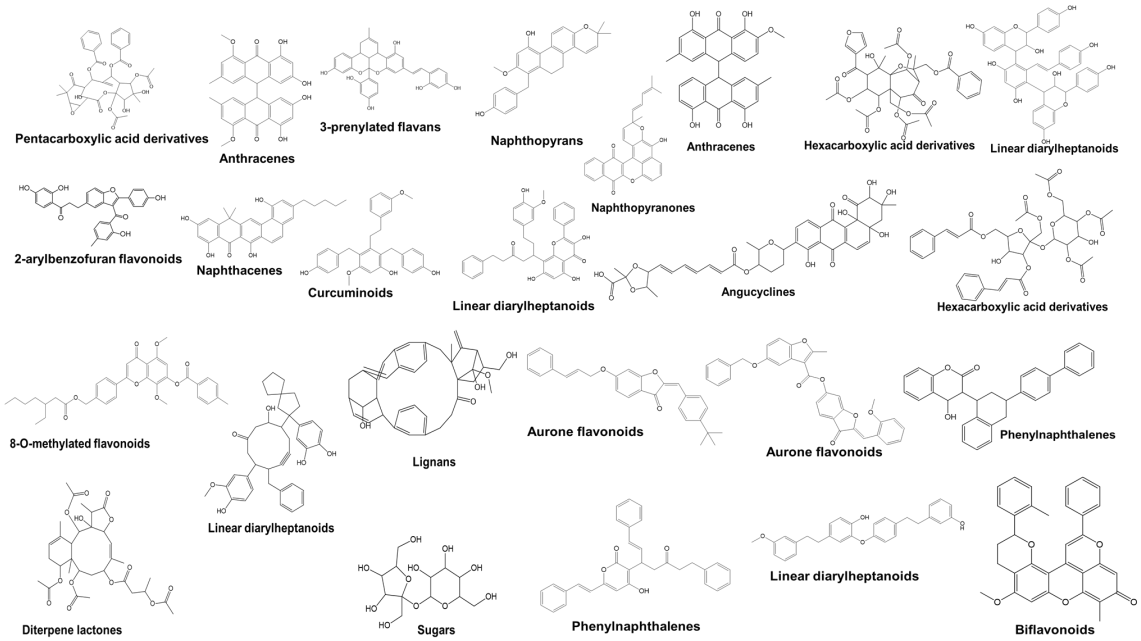

Figure 9. The LC-MS phytochemical analysis displays the structures of biologically active compounds identified in *W.salutaris* crude leaf extracts. ChemDraw Ultra version 12.0 was used to illustrate the structures.

Table 2. The LC-MS chromatogram of phytochemicals identified in the crude leaf extract of *Warbugai salutaris,* with metabolites eluting between 4.47 and 13.94 minutes.

ID	Retention time (min)	Measured (m/z)	Compound name	Biological Activity	Molecular Formula	Ref
545	5.4	507.14468	2-arylbenzofuran flavonoids	Antioxidant, Anti-inflammatory	$C_{31}H_{24}O_7$	(uk *et at*., 2023).
605	5.464	563.17297	3-prenylated flavans	Anticancer, Cytotoxic	$C_{34}H_{28}O_8$	(Jantip *et al*., 2025)
435	7.079	455.18509	Naphthacenes	Antimicrobial, Antitumor	$C_{29}H_{28}O_5$	(Bermejo-Casadesús et al., 2025)
573	7.311	537.15637	Anthracenes	Cytotoxic, Antiproliferative	$C_{32}H_{26}O_8$	(Jakob *et al*., 2020)
315	7.473	405.22162	Linear diarylheptanoids	Antioxidant, Anti-inflammatory	$C_{30}H_{30}O$	(Fang *et al*., 2024).
327	7.761	413.17435	Naphthopyrans	Anti-inflammatory, Cytotoxic	$C_{27}H_{26}O_4$	(Ahmed Borik *et al*., 2023).
474	9.048	469.19977	Curcuminoids	Anticancer, Anti-inflammatory	$C_{30}H_{30}O_5$	(Kaur *et al*., 2024)
631	9.175	579.20422	Linear diarylheptanoids	Anti-inflammatory, Cytotoxic	$C_{35}H_{32}O_8$	(Hameed, 2021).
318	9.578	409.17892	Aurone flavonoids	Antioxidant, Anticancer	$C_{28}H_{26}O_3$	(kte, Ungureanu,

© 2026 by the author(s). Distributed under a Creative Commons CC BY license.

Preprints.org (www.preprints.org) | NOT PEER-REVIEWED | Posted: 25 March 2026 doi:10.20944/preprints202603.1998.v1

						and Zaharia, 2023).
572	9.802	531.14600	Aurone flavonoids	Anti-inflammatory, Cytotoxic	$C_{33}H_{24}O_7$	(Zhu *et al.*, 2025)
409	9.893	445.17993	Phenylnaphthalenes	Antiproliferative, anti-cancer	$C_{31}H_{26}O_3$	(Elrayess and Elshihawy, 2023)
494	10.749	475.19086	Linear diarylheptanoids	Anticancer, Anti-inflammatory	$C_{32}H_{28}O_4$	(Sudarshan, Yarlagadda and Sengupta, 2024)
394	11.486	439.18967	Lignans	Anticancer, Cytotoxic	$C_{29}H_{28}O_4$	(Esquivel-Campos *et al.*, 2022).
538	11.585	501.17010	Biflavonoids	Antiproliferative, anti-cancer, Cytotoxic	$C_{33}H_{26}O_5$	(Lima *et al.*, 2024)
452	11.592	461.13800	Naphthopyranones	Cytotoxic, Anticancer	$C_{30}H_{22}O_5$	(Weber, F *et al.*, 2024)
544	11.592	507.14429	Anthracenes	Cytotoxic, anti-cancer, Antiproliferative	$C_{31}H_{24}O_7$	(Sk *et al.*, 2025)
758	11.684	755.21619	Hexacarboxylic acid derivatives	Anti-inflammatory, anti-cancer, Cytotoxic	$C_{37}H_{40}O_{17}$	(Bharath *et al.*, 2021)
751	11.959	739.22125	Linear diarylheptanoids	Anticancer, Anti-inflammatory	$C_{44}H_{36}O_{11}$	(Motiur *et al.*, 2018)
748	12.986	735.22589	Angucyclines	Antimicrobial, Antitumor	$C_{38}H_{40}O_{15}$	(Liu *et al.*, 2025).
640	13.126	585.24927	8-O-methylated flavonoids	Anticancer, Cytotoxic	$C_{35}H_{38}O_8$	(Berim and Gang, 2016)
674	13.574	607.30713	Linear diarylheptanoids	Anticancer, Anti-inflammatory	$C_{39}H_{44}O_6$	(Maurent *et al.*, 2018).
619	13.588	575.27985	Lignans	Antiproliferative, anti-cancer, Cytotoxic	$C_{38}H_{40}O_5$	(Jang, Kim and Cho, 2022)
700	13.941	635.26794	Diterpene lactones	Cytotoxic, Antitumor	$C_{32}H_{44}O_{13}$	(Islam *et al.*, 2018)

© 2026 by the author(s). Distributed under a Creative Commons CC BY license.

Preprints.org (www.preprints.org) | NOT PEER-REVIEWED | Posted: 25 March 2026 doi:10.20944/preprints202603.1998.v1

246	13.377	341.10751	Sugars	Nutrient, not bioactive, anti-cancer	$C_{12}H_{22}O_{11}$	(Akl and Ahmed, 2023)

3. Discussion

This study systematically compared the therapeutic efficacy and mechanistic properties of crude *Warburgia salutaris* leaf extract, both in its unencapsulated form (WSN) and when encapsulated within liposomal carriers (WSE). The integration of complementary analytical techniques—Fourier-transform infrared (FTIR) spectroscopy, powder X-ray diffraction (PXRD), and dynamic light scattering (DLS), provided robust evidence for the successful encapsulation and compatibility of *W. salutaris* phytochemicals within the DPPC-cholesterol liposomal matrix. PXRD analysis revealed that the crude plant extracts are inherently amorphous, while the lipid carriers display semi-crystallinity. The encapsulated formulation retained both amorphous and semi-crystalline characteristics, indicating that the amorphous bioactive phytochemicals were stably integrated into the lipid matrix without significant alteration to their physical state. Such preservation of the amorphous phase is advantageous, as it can enhance the solubility and bioavailability of the encapsulated compounds.

FTIR spectroscopy further corroborated the successful encapsulation, showing spectral features characteristic of plant-derived functional groups, including O-H, ester C=O, P=O, and P-O-C. Subtle spectral shifts in these regions indicate the presence of non-covalent interactions, such as hydrogen bonding and van der Waals forces, between the phytochemicals and the lipid bilayer [52]. These interactions are likely to influence encapsulation efficiency, vesicle stability, and release kinetics, all of which are critical for the effective delivery of bioactive agents.

The DLS measurements demonstrated that the liposomal formulation exhibited an average particle size of 159.4 nm and a low polydispersity index (PDI = 0.1140), indicating a highly uniform population of nanoscale vesicles. Furthermore, the liposomes displayed a high positive zeta potential of +79.3 mV, reflecting strong electrostatic repulsion that prevents particle aggregation and supports long-term colloidal stability. These physicochemical attributes, together with the PXRD and FTIR findings, confirm that the liposomal formulation maintains both structural and chemical integrity, making it suitable for the efficient delivery of bioactive phytochemicals. The amorphous nature of the encapsulated compounds is of particular interest, as it is known to facilitate strong interactions with phospholipid headgroups, reduce crystallisation within vesicles, and improve both the stability and entrapment efficiency of bioactive molecules. These findings are consistent with previous studies that have highlighted the benefits of amorphous systems in enhancing the performance of liposomal drug delivery platforms.

In vitro cytotoxicity assays were performed to compare the potency of both WSN and WSE extracts on cellular metabolic activity on MCF-7 (human breast cancer) and Vero (African green monkey kidney epithelial) cell lines. IC_{50} values were determined for each extract, revealing a significant reduction in metabolic activity in MCF-7 cells for both WSN and WSE, with WSN exhibiting the lowest IC_{50}. These results indicate that *W. salutaris* extracts, whether encapsulated or not, possess cytotoxic effects against cancer cells, as evidenced by reduced mitochondrial dehydrogenase activity in the MTT assay. In contrast, both Vero and Raw 264.7 (murine macrophage-like) cells showed increased metabolic activity upon treatment with WSN and WSE, suggesting selective cytotoxicity towards cancer cells. The observed differences in therapeutic response between cancerous and non-cancerous cell lines may be explained by the Warburg effect, which describes the preferential use of glycolysis over oxidative phosphorylation by cancer cells for ATP production [53]. The decline in MCF-7 cell metabolic activity could be attributed to various cytotoxic compounds identified in the LC-MS analysis of *W. salutaris*, including 3-prenylated flavans, naphthopyrans, lignans, naphthopyranones, linear diarylheptanoids, aurone flavonoids, biflavonoids, anthracenes, diterpenes, and lactones—all of which have demonstrated cytotoxic activities.

Additionally, both WSN and WSE extracts were found to inhibit cell proliferation in MCF-7 cells at a concentration of 0.3 mg/mL, indicating potential antimetastatic properties. This effect may be

© 2026 by the author(s). Distributed under a Creative Commons CC BY license.

Preprints.org (www.preprints.org) | NOT PEER-REVIEWED | Posted: 25 March 2026 doi:10.20944/preprints202603.1998.v1

related to the presence of anthracenes, lignans, and phenylnaphthalenes, compounds known for their ability to inhibit cell proliferation and induce cytotoxicity in cancer models [54,55].To further elucidate the cellular effects, nuclear staining assays using DAPI and Propidium Iodide (PI) were conducted. *W. salutaris* treated cells showed positive staining with both stains DAPI and PI, indicating compromised nuclear integrity and chromatin disintegration. WSN treatment resulted in more intense fluorescence, suggesting that potent anti-tumour compounds such as naphthacenes, angucyclines, and diterpene lactones may induce apoptosis by allowing PI to access and stain nucleic material, producing a characteristic red fluorescence Chaundhry 2022. DAPI, on the other hand, readily binds to fragmented DNA, producing blue fluorescence and further confirming apoptotic activity.

Gene and protein expression analyses provided additional mechanistic insights. Quantitative PCR revealed that pro-apoptotic genes Bax and caspase-3 were upregulated in response to both WSN and WSE, while the anti-apoptotic gene Bcl-2 was downregulated. Protein assays confirmed the activation of key apoptotic mediators, including Bax, Bad, cleaved caspase-3, SMAC/Diablo, Trail R1/DR4, Trail R2/DR5, TNF RI/TNFRSF1A, Fas/CD95, FADD, and phosphorylated p53 (S15, S46), indicating the initiation of both intrinsic (mitochondrial) and extrinsic (death receptor) apoptotic pathways. While many cancer studies focus primarily on inducing cancer cell death, this work shifts attention to inflammation, an important component of the immune response that combats infections. However, studies of the cancer microenvironment have shown that inflammation can also stimulate cancer progression [56,57] Therefore, compounds that possess both anticancer and anti-inflammatory properties are highly desirable [58]. This provides a rationale for the use of crude extracts rather than isolated compounds, as crude extracts may contain multiple bioactive constituents capable of targeting both processes simultaneously [59].

The anti-inflammatory properties of the extracts were evaluated through their effects on LPS-induced reactive oxygen species (ROS) production in Raw 264.7 macrophages. Both WSN and WSE demonstrated the ability to inhibit LPS-induced ROS generation, with WSE showing superior efficacy. This suggests that encapsulation not only preserves but may enhance the bioactivity of anti-inflammatory constituents. The inhibition of ROS production is likely due to the presence of compounds such as 2-arylbenzofuran flavonoids, linear diarylheptanoids, naphthopyrans, curcuminoids, aurone flavonoids, and hexacarboxylic acid derivatives, all of which have established anti-inflammatory activities [60,61]. Interestingly, at the lowest tested concentration (0.125 mg/mL), WSN was observed to directly induce cell death more than WSE. This could be attributed to the rapid release and direct interaction of unencapsulated bioactive compounds with cellular targets, leading to swift cell membrane damage and death. In contrast, the liposomal-encapsulated WSE afforded a more controlled and gradual activation of apoptotic pathways, highlighting the potential of encapsulation for modulating drug release and reducing off-target effects. Such controlled delivery is particularly desirable for minimising toxicity and side effects while maximising therapeutic efficacy in clinical applications.

Taken together, these results demonstrate that both crude and liposomal-encapsulated *W. salutaris* extracts possess significant anti-cancer, anti-proliferative, pro-apoptotic, and anti-inflammatory activities. Encapsulation within liposomal carriers enhances the stability, bioavailability, and controlled release of bioactive compounds, potentially reducing cytotoxicity to normal cells while maintaining or improving efficacy against cancer cells. These findings provide a strong foundation for further in vitro and in vivo studies aimed at optimising delivery systems, elucidating mechanisms of action, and ultimately developing novel therapeutic strategies based on W. salutaris phytochemicals.

4. Materials and Methods

Warbugia salutaris was selected based on ethnobotanical literature and its material collected in the gardens of Lowveld South African National Botanical Institute (SANBI), Mbombela, South Africa (25°27′57″S, 30°59′07″E). The plant specimens were then authenticated by a taxonomist in the

© 2026 by the author(s). Distributed under a Creative Commons CC BY license.

Preprints.org (www.preprints.org) | NOT PEER-REVIEWED | Posted: 25 March 2026 doi:10.20944/preprints202603.1998.v1

Department of Biology and Environmental Sciences at the Sefako Makgatho Health Sciences University. The leaves and stems of the plant were dried at room temperature and ground to a fine powder using a (POLYMIX® PX-MFC 90 D high-frequency impact mill, Kinematica AG, Switzerland). Plant material extracts were prepared according to the method described by Eloff (1998). 23 Briefly, approximately 20 g of each milled plant material was extracted with 200 mL of an equal mixture of dichloromethane and methanol (50/50) and shaken for 24 hours at room temperature. The extracts were then filtered through a Whatman No. 1 filter paper (Whatman No. 1, Boeco Qualitative filter, grade 3 hw 125 mm, Hamburg, Germany), followed by solvent evaporation using a rotary evaporator (Stuart RE300 Rotary Evaporator, Stuart, UK; supplied by Lasec). The dried extracts were stored in airtight containers at 4 °C.

4.1. Synthesis of Liposomal Nanoparticles

Liposomes were manufactured using thin-film hydration, following the method of Umbarkar et al. (2021), with minor modifications. In a clean round-bottom flask, 10 mL of methanol was used to dissolve phospholipids (dipalmitoyl phosphatidylcholine (DPPC), 100 mg) and cholesterol (10 mg, for membrane stability), along with the leaf extract of *W. salutaris* (10 mg). The mixture was placed in a rotary evaporator, and the solvent was removed under reduced pressure at ~45 °C. This formed a uniform, thin lipid layer on the inside surface of the flask. Subsequent vacuum drying removed any residual solvent. Ten millilitres of phosphate-buffered saline (PBS) was added to the lipid film. The temperature exceeded the phase transition point of DPPC (~50 °C), and the mixture was gently agitated to form multilamellar vesicles. Probe sonication was used for 5-10 minutes to reduce liposome size, producing small, uniform unilamellar vesicles. The liposomes were placed in sterile vials and stored at 4 °C until needed.

4.2. FTIR Spectroscopy

The FTIR spectra of the plant extracts, liposomal encapsulation, and liposomes were analysed using the Cary 630 Four Transform spectrophotometer (Agilent Technologies, California, United States of America) and subsequent analysis with OriginPro™ (OriginLab Corporation, Massachusetts, United States of America). An amount of 6g of lyophilised sample was placed on a diamond crystal and examined within the wavenumber range of 400-4000 cm^{-1} at 2 mm/s, with a resolution of 4 cm^{-1} at room temperature. FTIR spectra were recorded for the samples analysed. The analysis enables the identification of key biomolecules and provides insight into interactions between plant-derived phytochemicals and phospholipid vesicles during liposomal encapsulation.

4.3. Powder X-Ray Diffraction (pXRD)

Powder X-ray diffraction pattern was employed using a D2 Phaser XE-T Edition instrument (Bruker, Massachusetts, United States of America). The instrument used was a Bruker AXS diffractometer with CuKα radiation (λ = 1.54056 Å) over $20° \leq 2\theta \leq 80°$, operating at 40 kV and 40 mA. The divergent slit was set to 0.2 mm, and monochromator scanning was performed at 2 °/minute with a step size of 0.025 ° and a step time of 1 second. The lyophilised sample was positioned on the sample holder and aligned to ensure it fit completely. The average crystallite size of the sample was estimated using the Scherrer equation, which relates the broadening of the diffraction peaks to the size of coherently diffracting domains according to the expression: $0.9\lambda/d = B\cos\theta$

where λ is the wavelength of the X-ray radiation, B is the full width at half maximum of the diffraction peak (in radians), θ is the Bragg angle, and 0.9 is the shape factor (K) that accounts for crystallite morphology. This relation indicates that peak broadening (B) increases inversely with crystallite size (d), providing a means to estimate nanoscale domain dimensions from PXRD data.

4.4. Zeta Potential

© 2026 by the author(s). Distributed under a Creative Commons CC BY license.

Preprints.org (www.preprints.org) | NOT PEER-REVIEWED | Posted: 25 March 2026 doi:10.20944/preprints202603.1998.v1

The formulated liposomes loaded with plant extracts were analysed using Nano-wave II Zeta-sizer (Micotec, Pennsylvania, United States of America). Ten millilitres of the liposomal encapsulated extract was diluted with 100 mL of distilled water before analysis, followed by ultrasonication to achieve homogeneity. The sample was transferred into a 1.5 mL Eppendorf tube, and a sonication probe was introduced for 10 minutes at 25 °C.

4.5. Cell Culture

Breast cancer cells (MCF-7), kidney cells (Vero), and macrophages (Raw 264.7) were obtained from Cellonex (Pty) Ltd., Johannesburg, South Africa, and cultured separately in T75 flasks (Sigma-Aldrich (Pty) Ltd., an affiliate of Merck KGaA. Dulbecco's Modified Eagle Medium (DMEM) and Roswell Park Memorial Institute Medium (RPMI-1640) were used for cell maintenance (Sigma-Aldrich (Pty) Ltd., an affiliate of Merck KGaA). Each medium contained 10% foetal bovine serum (FBS), 1% penicillin-streptomycin antibiotic cocktail, and 5% L-glutamine (Sigma-Aldrich (Pty) Ltd., an affiliate of Merck KGaA). Cultures were maintained at 37 °C in incubators with 5% CO_2 and high humidity. Culture medium was replaced every 2 to 3 days until cells reached approximately 80 to 90% confluence. A Nikon Eclipse TS100 light microscope (Nikon Corporation, Tokyo, Japan) was used to systematically assess cell morphology, viability, and mycoplasma infection status. In subsequent experiments, cells were seeded at a density of 1×10^5 cells/ml into 96-well plates.

4.6. Cell Viability Assay

The MTT assay was used to evaluate cellular metabolic activity in selected cells following a method described by Monama et al. (2025). Cultured MCF-7, Vero and Raw 264.7 cells were seeded in 96-well plates at a density of 1×10^5 cells/mL and allowed to adhere overnight under standard conditions. The cells were exposed to various concentrations of extracts, ranging from 0.25 to 25 mg/ml. Doxorubicin and hydrogen peroxide served as positive controls, while untreated cells acted as negative controls. After a 24-hour incubation at 37 °C, 20 µL of 5 mg/mL MTT reagent was added to each well. The plates were incubated for a further 4 hours to allow mitochondrial dehydrogenases in viable cells to reduce MTT to purple formazan crystals. Subsequently, the medium was removed, and the cells were gently rinsed once with pre-warmed PBS (pH 7.4). Intracellular formazan was dissolved in acidic isopropanol, and absorbance was read at 570 nm using a GloMax® Multi-detection system (Promega, USA). Results are expressed as mean ± standard deviations of two independent triplicate experiments.

$$Percentage\ viability\ (\%) = \frac{Absorbance\ of\ treated\ cells}{Absorbance\ of\ untreated\ cells} x\ 100$$

4.7. Anti-Metastatic Assay in MCF-7 Cells

The anti-metastatic activity of WSN and WSE leaf extracts was evaluated using an in vitro scratch assay. MCF-7 cells were cultured in RPMI medium supplemented with 10% fetal bovine serum (FBS), 5% L-glutamine, and 5% penicillin–streptomycin and incubated at 37 °C in a humidified atmosphere containing 5% CO_2 until reaching approximately 70–80% confluency. A straight scratch was created across the cell monolayer using a sterile 10 µL pipette tip. The cells were gently washed with phosphate-buffered saline (PBS) to remove detached cells and debris. Cells were then treated with WSN and WSE extracts at a concentration of 0.3 mg/mL. Untreated cells served as the negative control, while cells treated with doxorubicin were used as the positive control. Images of the wound area were captured at 0 h and 24 h using an inverted microscope (Nikon Eclipse TS100) at 10× magnification. The same region of the scratch was imaged at both time points.

4.8. H2DCF-DA Assay

Reactive oxygen species (ROS) were evaluated in macrophage cells (RAW 264.7) using a modified protocol based on Chen et al. (2013). The cells were seeded at a density of 6 × 104 cells per

© 2026 by the author(s). Distributed under a Creative Commons CC BY license.

Preprints.org (www.preprints.org) | NOT PEER-REVIEWED | Posted: 25 March 2026 doi:10.20944/preprints202603.1998.v1

well in a 96-well plate and incubated at 37 °C in 5% CO2 for 24 hours. After incubation, cells were treated with 100 µL of a 125 µg/mL dichloromethane: methanol (50/50) extract of W. salutaris and with lipopolysaccharide (LPS) (10 µg/mL) as a positive control. After incubation for 24 hours, 10 µM H2DCF-DA was added and incubated in the dark for an additional 30 minutes. Fluorescence was read using a microplate reader at 485 nm (excitation) and 535 nm (emission). The Raw 264.7 cells were also cultivated on coverslips in 6-well plates and received identical treatments. The slides were then prepared for visualisation, and images showing the effect of LPS-induced ROS generation by extracts were captured using Zoe fluorescent microscopy with the H2DCF-DA dye.

4.9. RNA Extraction and Purification

To evaluate the transcriptional response of MCF-7 breast cancer cells to EA/DCM extracts, total RNA was isolated following a 24-hour treatment period at a concentration of 1000 µg/mL. The extraction process utilised the GeneJET RNA Purification Kit (Thermo Scientific) in accordance with the manufacturer's instructions. Briefly, approximately 1.0 x 10^5 cells were harvested via centrifugation at 1000 rpm for 5 minutes. The resulting cell pellets were washed with sterile phosphate-buffered saline (PBS) to eliminate residual culture media and centrifuged again. The washed cells were resuspended in 600 µL of lysis buffer supplemented with *ß*-mercaptoethanol to stabilise the RNA. A 250 µL aliquot of this lysate was then homogenised with 360 µL of absolute ethanol. The mixture (700 µL) was loaded onto a GeneJET purification column and centrifuged at 12,000 rpm for 1 minute. Contaminants were removed through a series of wash steps: first with 700 µL of Wash Buffer 1, followed by a 600 µL wash and a final 250 µL wash with Wash Buffer 2, each followed by centrifugation at 12,000 rpm. Finally, the purified RNA was eluted into a sterile tube using 100 µL of nuclease-free water and immediately processed for downstream applications.

4.10. First-Strand cDNA Synthesis

The purity and concentration of the isolated total RNA were quantified using a Qubit 2.0 Fluorometer (Invitrogen Life Technologies, Singapore). For the synthesis of complementary DNA (cDNA), 0.1–0.5 µg of total RNA served as the template. Reverse transcription was performed using the RevertAid First Strand cDNA Synthesis Kit (Thermo Scientific). The synthesis reaction was conducted in a total volume of 20 µL, comprising 1 µL of template RNA and a master mix of reagents as detailed in Table 6.1. This mixture included Oligo(dT) primers, 5X reaction buffer, RiboLock RNase Inhibitor, 10 mM dNTP mix, and RevertAid M-MuLV Reverse Transcriptase. After gentle homogenization and brief centrifugation, the samples were incubated at 42 °C for 60 minutes to facilitate primer extension. The enzymatic reaction was subsequently terminated by thermal denaturation at 70 °C for 5 minutes. The resulting cDNA was stored at appropriate temperatures for subsequent PCR analysis.

4.11. Polymerase Chain Reaction (PCR)

Polymerase Chain Reaction (PCR) amplification was performed according to the protocol outlined by Gaikwad *et al*. (2017). Reactions were performed on a QuantStudio™ 3 thermal cycler (Applied Biosystems, Thermo Fisher Scientific, Waltham, MA, USA). The cycling conditions included an initial denaturation at 95 °C for 10 minutes, followed by 30 cycles of denaturation at 95 °C for 30 seconds, primer annealing at 61 °C for 30 seconds, and extension at 72 °C for 60 seconds. A final extension step of 72 °C for 7 minutes was followed by a hold at 4 °C. PCR products were separated on a 1.5% agarose gel containing 0.5 µg/mL ethidium bromide, visualised with a Chemidoc imaging system (Bio-Rad Laboratories (Pty) Ltd., South Africa). Densitometric analysis quantified band intensities normalised to GAPDH expression, measured mRNA levels relative to other genes, and reported results as fold changes. Data analysis was performed using GraphPad Prism 8.4, and results were shown as mean fold increase ± SEM for gene expression percentages. The primer sequences used are listed in Table 3.

© 2026 by the author(s). Distributed under a Creative Commons CC BY license.

Preprints.org (www.preprints.org) | NOT PEER-REVIEWED | Posted: 25 March 2026 doi:10.20944/preprints202603.1998.v1

Table 3. The primer sequences for gene amplification of GAPDH, *caspase-3*, *bax* and *bcl-2*.

Gene	Primer sequence
caspase-3	Forward: 5′CCATGGGTAGCAGCCTCCTTC 3′ Reverse: 3′ TGCGCTGCTCTGCCTTCT 5′
Bax	Forward: 5′TCCCCCCAGAGGTCTTTT 3′ Reverse: 3′CGGCCCCAGTTGAAGTTG 5′
bcl-2	Forward: 5′CTGCACCTGACGCCCTTCACC 3′ Reverse: 3′CACATGACCCCACCGAACTCAAAGA 5′
GAPDH	Forward: 5′TGCGCTGCTGCTCTGCCTTCT 3′ Reverse: 3′CCATGGGTAGCAGCTCCTTC 5′

4.12. Annexin V-FITC and Propidium Iodide (PI), Analysis by Muse® Cell Analyser

The quantification of apoptotic cell populations was conducted via flow cytometry, following the dual-staining protocol described by Kocyigit et al. (2018). The MCF-7 cell lines were exposed to different concentrations of EA/DCM fractioned leaf extracts of *W. salutaris* for four hours. After treatment, cells were harvested with a sterile cell scraper, centrifuged at 800 rpm for 10 minutes, and washed twice with 1 mL of ice-cold phosphate-buffered saline (PBS). The cells were then fixed in 4% paraformaldehyde at 4 °C overnight. For staining, cells were incubated in the dark at 37 °C for 30 minutes with 500 µL of a solution containing propidium iodide, RNase A, and buffer. Following incubation, cell viability and counting were performed using the Guava Muse® Cell Analyser (Luminex Corporation, USA) to quantify apoptotic cells, cell death, and viable cells. Cells cultured in 6-well plates were used in a single experiment.

4.13. Human Apoptosis Proteome Array

The protein expression assay was prepared according to the manufacturer's instructions for the Proteome Profiler Human Apoptosis Array Kit (Cat. No. ARY009, R&D Systems, Minneapolis, MN, USA), and the manufacturer's instructions were adhered to throughout the process. Each well of a 4-well multi-dish was filled with 2 mL of Array Buffer 1, which served as the blocking buffer. The arrays were carefully removed from their protective sheets using flat-tip tweezers and placed into each well with the array number facing upwards. After incubation on a rocking platform shaker for one hour, cell lysates were diluted in Array Buffer 1, and the final volume was adjusted to 1.5 ml with lysis buffer. The maximum volume of each array was 250 µL. The blocking buffer was discarded, and samples were added to the wells. The plates were gently agitated and incubated overnight at 2-8 °C. The arrays were washed three times with 1X Wash Buffer, then incubated for 1 hour with a diluted detection antibody cocktail. After several washes, the arrays were incubated in diluted Streptavidin-HRP for 30 minutes. After the final wash, the membranes were dried, and 1 mL of Chemi reagent mix was evenly applied and left for 1 minute under plastic sheet protectors to ensure complete coverage. The excess reagent was wiped with absorbent wipes. The membranes, each labelled with its identifying number and facing up, were placed in an autoradiography cassette and covered with plastic. An X-ray film was used to expose the membranes for 1-10 minutes, with varying exposure times to enhance signal detection.

4.14. Liquid Chromatography-Mass Spectrometry (LC-MS)

The phytochemical profile of the crude leaf extract of W. salutaris was analysed using a Waters Acquity UPLC system and a Synapt G2 QTOF mass spectrometer (Waters, Milford, MA, USA) with an electrospray ionisation source operated in negative mode. Approximately 50 mg of dried, powdered leaf material was mixed with 1 mL of 50% methanol containing 0.1% formic acid. The mixture was vortexed, sonicated for 1 hour, and then centrifuged at 3000 × g for 10 minutes. The supernatant was filtered through a 0.22 µm syringe filter. Each sample underwent three analyses. Separation was achieved on an Acquity BEH C18 column (2.1 × 100 mm, 1.7 µm) maintained at 55 °C,

© 2026 by the author(s). Distributed under a Creative Commons CC BY license.

Preprints.org (www.preprints.org) | NOT PEER-REVIEWED | Posted: 25 March 2026 doi:10.20944/preprints202603.1998.v1

using a mobile phase of water (0.1% formic acid, A) and acetonitrile (0.1% formic acid, B) at a flow rate of 0.35 mL/min. The gradient programme was: 0-0.5 min, 100% A; 0.5-3 min, 22% B; 3-7 min, 44% B; 7-12 min, 100% B, held for 2 minutes, then re-equilibrated to initial conditions by 15 minutes. The injection volume was 3 μL, and the eluate was directed through a PDA detector before mass spectrometry analysis. Data were acquired in MSE mode from m/z 150 to 1500 by alternation between low energy (4 V) and high energy (40-100 V) to capture precursor and fragment ions. The source parameters included a capillary voltage of 2.5 kV, a cone voltage of 15 V, and a desolation gas flow rate of 650 L/h at 275 °C. Sodium formate served as the calibration standard, while leucine enkephalin was used as the lock mass. MS-DIAL software was used to identify and align peaks in the raw data. Subsequently, MS-FINDER was utilised to investigate the exact masses, isotopic patterns, retention characteristics, and in silico fragmentation of compounds in relation to metabolome databases. A catechin calibration curve (0.2-5 mg/L) was used for semi-quantification, and features that remained consistent across three injections were retained for further analysis.

4.15. Statistical Analysis

Statistical analysis was performed using GraphPad Prism version 8.4. All experimental results were expressed as mean ± standard deviation (SD) from at least three independent experiments performed in triplicate, and significance was determined by one-way ANOVA with nonlinear regression for IC50 values ($p < 0.05$).

5. Conclusion

In conclusion, this study robustly demonstrates that crude leaf extracts *of Warburgia salutaris*, as well as their liposomal-encapsulated forms, exhibit pronounced anti-cancer, anti-tumour, anti-proliferative, and anti-inflammatory activities. The results underscore the potential of liposomal nanocarriers not only to enhance the stability and controlled release of bioactive compounds but also to improve selective cytotoxicity towards cancer cells while minimising adverse effects on normal cells. These findings align with and extend prior evidence supporting the therapeutic promise of amorphous, encapsulated phytochemicals in targeted drug delivery systems.

Importantly, the differential effects observed in cancerous versus non-cancerous cell lines, the significant inhibition of inflammatory responses, collectively provide a comprehensive mechanistic rationale for further development of *W. salutaris*-based therapeutics. Moving forward, our research will systematically investigate both isolated bioactive constituents and liposomal bioencapsulated extracts in advanced in vitro and in vivo models, with a specific focus on their efficacy in reversing tumour progression and mitigating inflammation, particularly in murine systems. Additional studies are planned to characterise drug release kinetics and permeability, thereby enabling a detailed assessment of bioavailability and pharmacodynamic profiles under physiologically relevant conditions.

Altogether, these efforts will contribute critical insights into the optimisation of delivery platforms, the elucidation of molecular mechanisms, and the rational design of innovative phytochemical-based therapies. Ultimately, this work lays a strong foundation for the translational development of W. salutaris as a novel candidate for safe and effective cancer and inflammation management, with the potential to inform broader strategies in natural product drug discovery and nanomedicine.

Author Contributions: Conceptualisation D.M.T, M. P. M and L.J.S. methodology, D.M.T, M.S.M, E.H.M., M.P.M. J.B.N. R.T.M.; software, D.M.T., R.T. M., J.B.N., and M.S.M.; validation L.J.S., M.P.M., B.A.W., A.H.K.,S.S.G and E.H.M.; formal analysis D.M.T., M.P.M., R.T.M and L.J.S.; investigation D.M.T and M.P.M.; resources; L.J.S., R.T.M., A.H.K., and B.A.W., data curation; D.M.T., R.T.M., and M.P.M.; original draft writing D.M.T.; review and editing, L.J.S., S.SG., B.A.W., M.P.M., E.H.M., and J.B.N.; visualisation, R.T.M., A.H.K., and J.B.N.; supervision, S.SG., A.H.K and L.J.S., project administration L.J.S.; Funding acquisition A.H.K. All authors read and agreed to the published version of the manuscript.

© 2026 by the author(s). Distributed under a Creative Commons CC BY license.

Preprints.org (www.preprints.org) | NOT PEER-REVIEWED | Posted: 25 March 2026 doi:10.20944/preprints202603.1998.v1

Funding: This research was funded by the Department of Biochemistry and Biotechnology, under the School of Science and Technology at Sefako Makgatho Health Science University, in collaboration with the Department of Biomedical Science, Faculty of Science, at Tshwane University of Technology.

Institutional Review Board Statement: The study was conducted in accordance with the Declaration of Helsinki and approved by the Sefako Makgatho Health Sciences University research committee (SMUREC) of Sefako Makgatho Health Sciences University (Reference No: SMUREC/S/414/2024: PG on 09/2024, Project ID: 2392).

Informed Consent Statement: Not applicable.

Data Availability Statement: The original contributions presented in this study are included in the article/supplementary material. Further inquiries can be directed to the corresponding author(s).

Acknowledgments: The authors would like to express their sincere gratitude to the Department of Biomedical Sciences, Tshwane University of Technology, Arcadia Campus, the Department of Biochemistry and Microbiology, University of Limpopo, and the Department of Pharmaceutical Sciences, School of Pharmacy, Sefako Makgatho Health Sciences University, Pretoria, South Africa, for generously providing laboratory space and resources that made this work possible. Further acknowledge the National Research Fund (NRF) (ORCiD 0000-0002-9960-5565) for financial support.

Conflicts of Interest: The Authors declare no conflict of interest with the data contained in the manuscript.

Abbreviations

The following abbreviations are used in this manuscript:

Bax, Bcl-2-associated X protein
Bcl-2, B-cell lymphoma 2
DLS, Dynamic Light Scattering
FTIR, Fourier Transform Infrared Spectroscopy
H_2DCF-DA, 2′,7′-Dichlorodihydrofluorescein diacetate
IC_{50}, Half-maximal inhibitory concentration
LC–MS, Liquid Chromatography–Mass Spectrometry
LPS, Lipopolysaccharide
PDI, Polydispersity Index;
PXRD, Powder X-ray Diffraction
RT-PCR, Reverse Transcription Polymerase Chain Reaction
WSE, *Warburgia salutaris* liposomal-encapsulated crude leaf extract
WSN, *Warburgia salutaris* unencapsulated crude leaf extract

References

1. Yadav AR, Mohite SK. Cancer-A silent killer: An overview. *Asian Journal of Pharmaceutical Research*. 2020;10(3):213–216.
2. Santibáñez-Andrade M, Chirino YI, González-Ramírez I, Sánchez-Pérez Y, García-Cuellar CM. Deciphering the code between air pollution and disease: the effect of particulate matter on cancer hallmarks. *International journal of molecular sciences*. 2019;21(1):136.
3. Ali A, Manzoor MF, Ahmad N, et al. The burden of cancer, government strategic policies, and challenges in Pakistan: A comprehensive review. *Frontiers in nutrition*. 2022;9:940514.
4. Halperin DT. Coping with COVID-19: learning from past pandemics to avoid pitfalls and panic. *Global Health: Science and Practice*. 2020;8(2):155–165.
5. Finestone E, Wishnia J. Estimating the burden of cancer in South Africa. *SA Journal of Oncology*. 2022;6(0):220.
6. Hamdi Y, Abdeljaoued-Tej I, Zatchi AA, et al. Cancer in Africa: the untold story. *Frontiers in oncology*. 2021;11:650117.

© 2026 by the author(s). Distributed under a Creative Commons CC BY license.

Preprints.org (www.preprints.org) | NOT PEER-REVIEWED | Posted: 25 March 2026 doi:10.20944/preprints202603.1998.v1

7. Lombe DC, Mwamba M, Msadabwe S, et al. Delays in seeking, reaching and access to quality cancer care in sub-Saharan Africa: a systematic review. *BMJ open*. 2023;13(4):e067715.
8. Ndlovu BH. *Awareness, knowledge and experiences of women regarding cervical cancer in rural Kwazulu-Natal, South Africa*. Stellenbosch: University of Stellenbosch; 2011.
9. Goswami N. A dual burden dilemma: Navigating the global impact of communicable and non-communicable diseases and the way forward. *International Journal of Medical Research*. 2024;12(3):65–77.
10. Schirrmacher V. From chemotherapy to biological therapy: A review of novel concepts to reduce the side effects of systemic cancer treatment. *International journal of oncology*. 2019;54(2):407–419.
11. Tripathi D, Pandey P, Sharma S, Rai AK, BH MP. Advances in nanomaterials for precision drug delivery: Insights into pharmacokinetics and toxicity. *BioImpacts: BI*. 2024;15:30573.
12. Mao JJ, Pillai GG, Andrade CJ, et al. Integrative oncology: Addressing the global challenges of cancer prevention and treatment. *CA: a cancer journal for clinicians*. 2022;72(2):144–164.
13. Kutova OM, Guryev EL, Sokolova EA, Alzeibak R, Balalaeva IV. Targeted delivery to tumors: multidirectional strategies to improve treatment efficiency. *Cancers*. 2019;11(1):68.
14. Dehelean CA, Marcovici I, Soica C, et al. Plant-derived anticancer compounds as new perspectives in drug discovery and alternative therapy. *Molecules*. 2021;26(4):1109.
15. Hashim GM, Shahgolzari M, Hefferon K, Yavari A, Venkataraman S. Plant-Derived Anti-Cancer Therapeutics and Biopharmaceuticals. *Bioengineering*. 2024;12(1):7.
16. Salehi B, Fokou PVT, Yamthe LRT, et al. Phytochemicals in prostate cancer: from bioactive molecules to upcoming therapeutic agents. *Nutrients*. 2019;11(7):1483.
17. Ayaz M, Nawaz A, Ahmad S, et al. Underlying anticancer mechanisms and synergistic combinations of phytochemicals with cancer chemotherapeutics: potential benefits and risks. *Journal of Food Quality*. 2022;2022(1):1189034.
18. Viljoen A, Sandasi M, Fouche G, Combrinck S, Vermaak I. *The South African Herbal Pharmacopoeia: Monographs of Medicinal and Aromatic Plants*. Academic Press; 2022.
19. Kyriakoudi A, Spanidi E, Mourtzinos I, Gardikis K. Innovative Delivery Systems Loaded with Plant Bioactive Ingredients: Formulation Approaches and Applications. Plants 2021, 10, 1238. s Note: MDPI stays neutral with regard to jurisdictional claims in published …; 2021.
20. Leonard C, Chen W, Kamatou G. *Warburgia salutaris*. *The South African Herbal Pharmacopoeia*. Elsevier; 2023:531–556.
21. Garcia-Oliveira P, Otero P, Pereira AG, et al. Status and challenges of plant-anticancer compounds in cancer treatment. *Pharmaceuticals*. 2021;14(2):157.
22. Emeihe EV, Nwankwo EI, Ajegbile MD, Olaboye JA, Maha CC. Revolutionizing drug delivery systems: Nanotechnology-based approaches for targeted therapy. *Int J Life Sci Res Arch*. 2024;7(1):40–58.
23. Eloff J. Which extractant should be used for the screening and isolation of antimicrobial components from plants? *Journal of ethnopharmacology*. 1998;60(1):1–8.
24. Umbarkar M, Thakare S, Surushe T, Giri A, Chopade V. Formulation and evaluation of liposome by thin film hydration method. *J Drug Deliv Ther*. 2021;11(1):72–76.
25. Jovanović AA, Balanč B, Petrović PM, et al. Design and characterization of liposomal-based carriers for the encapsulation of rosa canina fruit extract: in vitro gastrointestinal release behavior. *Plants*. 2024;13(18):2608.
26. Ajeeshkumar KK, Aneesh PA, Raju N, Suseela M, Ravishankar CN, Benjakul S. Advancements in liposome technology: Preparation techniques and applications in food, functional foods, and bioactive delivery: A review. *Comprehensive Reviews in Food Science and Food Safety*. 2021;20(2):1280–1306. doi:https://doi.org/10.1111/1541-4337.12725
27. Bononi G, Masoni S, Di Bussolo V, Tuccinardi T, Granchi C, Minutolo F. Historical perspective of tumor glycolysis: a century with Otto Warburg. Elsevier; 2022:325–333.
28. Jakob CH, Dominelli B, Schlagintweit JF, et al. Improved antiproliferative activity and fluorescence of a dinuclear gold (I) bisimidazolylidene complex via anthracene-modification. *Chemistry–An Asian Journal*. 2020;15(24):4275–4279.
29. Hameed R. Diarylheptanoids: Potent Anticancer Agents. *Clinical Cancer Drugs*. 2021;8(1):18–26.

© 2026 by the author(s). Distributed under a Creative Commons CC BY license.

Preprints.org (www.preprints.org) | NOT PEER-REVIEWED | Posted: 25 March 2026 doi:10.20944/preprints202603.1998.v1

30. Esquivel-Campos A, Pérez-Gutiérrez S, Sánchez-Pérez L, Campos-Xolalpa N, Pérez-Ramos J. Cytotoxicity and Antitumor Action of Lignans and Neolignans. *Secondary Metabolites-Trends and Reviews*. 2022;
31. Ahmed Borik RM, Amri NJ, Mukhrish YE, et al. Design, synthesis, reactions, molecular docking, antitumor activities of novel naphthopyran, naphthopyranopyrimidines, and naphthoyranotriazolopyrimidine derivatives. *Current Organic Chemistry*. 2023;27(19):1717–1727.
32. Lima CAd, Maquedano LK, Jaalouk LS, Santos DCd, Longato GB. Biflavonoids: preliminary reports on their role in prostate and breast cancer therapy. *Pharmaceuticals*. 2024;17(7):874.
33. Weber F, Weber A, Schmitt L, et al. From the Total Synthesis of Semi–Viriditoxin, Semi–Viriditoxic Acid and Dimeric Naphthopyranones to their Biological Activities in Burkitt B Cell Lymphoma. *Chemistry–A European Journal*. 2024;30(25):e202400559.
34. Jantip P, Singh CK, Klu YAK, Ahmad N, Bolling BW. Peanut skin polyphenols inhibit proliferation of leukemia cells in vitro, and its A-type procyanidins selectively pass through a Caco-2 intestinal barrier. *Journal of Food Science*. 2025;90(2):e70018.
35. Sk S, Chakrovorty A, Samadder A, Bera M. A family of zinc compounds of an anthracene-appended new multifunctional organic scaffold as potent chemotherapeutics against cervical cancer. *Materials Advances*. 2025;6(4):1478–1496.
36. Zhu Q, Zheng X, Tan Y, Luo Z, Yao X, Chen H. Biological Activities of Aurones: A Brief Summary. *Mini-Reviews in Organic Chemistry*. 2025;22(2):226–243.
37. Jang WY, Kim M-Y, Cho JY. Antioxidant, anti-inflammatory, anti-menopausal, and anti-cancer effects of lignans and their metabolites. *International journal of molecular sciences*. 2022;23(24):15482.
38. Elrayess RA, Elshihawy H. Naphthalene: an overview. *Records of Pharmaceutical and Biomedical Sciences*. 2023;7(1):145–153.
39. Bermejo-Casadesús C, Gonzalo-Navarro C, Organero JA, et al. New encapsulated bis-cyclometalated Ir (III) complexes with very potent anticancer PDT activity. *Inorganic Chemistry Frontiers*. 2025;12(22):7304–7332.
40. Liu H-S, Chen H-R, Huang S-S, Li Z-H, Wang C-Y, Zhang H. Bioactive Angucyclines/Angucyclinones Discovered from 1965 to 2023. *Marine Drugs*. 2025;23(1):25.
41. Monama LV, Tswaledi DL, Hadzhi TM, et al. Identification of Bioactive Compounds in *Warburgia salutaris* Leaf Extracts and Their Pro-Apoptotic Effects on MCF-7 Breast Cancer Cells. *International Journal of Molecular Sciences*. 2025;26(16):8065.
42. Mustafa M, Ahmad R, Tantry IQ, et al. Apoptosis: a comprehensive overview of signaling pathways, morphological changes, and physiological significance and therapeutic implications. *Cells*. 2024;13(22):1838.
43. Wani AK, Akhtar N, Mir TuG, et al. Targeting apoptotic pathway of cancer cells with phytochemicals and plant-based nanomaterials. *Biomolecules*. 2023;13(2):194.
44. Maurent K, Vanucci-Bacque C, Baltas M, Negre-Salvayre A, Auge N, Bedos-Belval F. Synthesis and biological evaluation of diarylheptanoids as potential antioxidant and anti-inflammatory agents. *European Journal of Medicinal Chemistry*. 2018;144:289–299.
45. Motiur Rahman A, Lu Y, Lee H-J, et al. Linear diarylheptanoids as potential anticancer therapeutics: synthesis, biological evaluation, and structure–activity relationship studies. *Archives of pharmacal research*. 2018;41(12):1131–1148.
46. Bharath B, Perinbam K, Devanesan S, AlSalhi MS, Saravanan M. Evaluation of the anticancer potential of Hexadecanoic acid from brown algae Turbinaria ornata on HT–29 colon cancer cells. *Journal of Molecular Structure*. 2021;1235:130229.
47. Sudarshan K, Yarlagadda S, Sengupta S. Recent advances in the synthesis of diarylheptanoids. *Chemistry–An Asian Journal*. 2024;19(15):e202400380.
48. Covarrubias A, Byles V, Horng T. ROS sets the stage for macrophage differentiation. *Cell research*. 2013;23(8):984–985.
49. Xie Y, Liu F, Wu Y, et al. Inflammation in cancer: therapeutic opportunities from new insights. *Molecular cancer*. 2025;24(1):51.
50. Aggarwal V, Tuli HS, Varol A, et al. Role of reactive oxygen species in cancer progression: molecular mechanisms and recent advancements. *Biomolecules*. 2019;9(11):735.

© 2026 by the author(s). Distributed under a Creative Commons CC BY license.

Preprints.org (www.preprints.org) | NOT PEER-REVIEWED | Posted: 25 March 2026 doi:10.20944/preprints202603.1998.v1

51. Nwosu SN, Obagbemisoye OV, Onuba CO, Balogun SE. Advances in Anticancer Drug Discovery: Exploring the Untapped Potential of Natural Products for Targeted Therapies. *Journal of Advances in Medical and Pharmaceutical Sciences*. 2024;26(11):1–22.
52. Karonen M. Insights into polyphenol–lipid interactions: Chemical methods, molecular aspects and their effects on membrane structures. *Plants*. 2022;11(14):1809.
53. López-Lázaro M. The warburg effect: why and how do cancer cells activate glycolysis in the presence of oxygen? *Anti-Cancer Agents in Medicinal Chemistry-Anti-Cancer Agents)*. 2008;8(3):305–312.
54. Mukhija M, Joshi BC, Bairy PS, Bhargava A, Sah AN. Lignans: a versatile source of anticancer drugs. *Beni-suef university journal of basic and applied sciences*. 2022;11(1):76.
55. Chang C-F, Ke C-Y, Wu Y-C, Chuang T-H. Structure-activity relationship of synthetic 2-phenylnaphthalenes with hydroxyl groups that inhibit proliferation and induce apoptosis of MCF-7 cancer cells. *PLoS One*. 2015;10(10):e0141184.
56. Zhao H, Wu L, Yan G, et al. Inflammation and tumor progression: signaling pathways and targeted intervention. *Signal transduction and targeted therapy*. 2021;6(1):263.
57. Greten FR, Grivennikov SI. Inflammation and cancer: triggers, mechanisms, and consequences. *Immunity*. 2019;51(1):27–41.
58. Luo R, Yue Z, Yang Q, et al. In situ repolarization of tumor-associated macrophages with synergic nanoformulation to reverse immunosuppressive TME in mouse breast cancer for cancer therapy. *Journal of Pharmaceutical Analysis*. 2024;14(8):100941.
59. Altemimi A, Lakhssassi N, Baharlouei A, Watson DG, Lightfoot DA. Phytochemicals: Extraction, isolation, and identification of bioactive compounds from plant extracts. *Plants*. 2017;6(4):42.
60. Edwards RL, Luis PB, Varuzza PV, et al. The anti-inflammatory activity of curcumin is mediated by its oxidative metabolites. *Journal of Biological Chemistry*. 2017;292(52):21243–21252.
61. Rani P, Dhillon S, Kumari G, et al. 2-Arylidene-6-methyl-2H-furo [3, 2-c] pyran-3, 4-diones: Design, synthesis, and evaluation of Anti-inflammatory, Anti-malarial, and Anti-cancer efficacy. *Journal of Molecular Structure*. 2025;1340:142371.

Disclaimer/Publisher's Note: The statements, opinions and data contained in all publications are solely those of the individual author(s) and contributor(s) and not of MDPI and/or the editor(s). MDPI and/or the editor(s) disclaim responsibility for any injury to people or property resulting from any ideas, methods, instructions or products referred to in the content.

© 2026 by the author(s). Distributed under a Creative Commons CC BY license.